Geoinformatics, vol.15, no.4, pp.207-219, 2004

ARTICLE

SIMULATION OF HIMALAYAN MAJOR THRUSTS BY FINITE ELEMENT METHOD

M. Farhad HOWLADAR * and Daigoro HAYASHI *

* Tectonic Laboratory, Department of Physics and Earth Sciences, University of the Ryukyus, Nishihara, Okinawa 903-0213, Japan. E-mail: mfhowladar75@hotmail.com ; daigoro@sci.u-ryukyu.ac.jp

(Received: 17 May 2004; Accepted: 08 November 2004)

Abstract : The Himalayan mountain system developed from the powerful earth movements which occurred as the Indian plate pressed against the Eurasian continental plate. A series of elastic finite element models are presented to examine the development of major thrusts (MCT, MBT and MFT) in the central Himalaya. Balanced geologic profiles of the central Himalaya which are modified from Johnson's profiles (2002) are used for the purpose under plane strain condition. The convergent rate of India has changed 10 cm/a at 40 Ma, 5 cm/a at 20 Ma and 2 cm/a at 10 Ma. Results show that the horizontal compressive stress σ_1 leads to the development of thrust faults in the Ththys Himalaya, Higher Himalaya, Lesser Himalaya, Sub-Himalaya and incipient zones of MCT, MBT and MFT. Especially, the thrust faults are highly concentrated within the whole area of the incipient zones, which influenced the formation of MCT, MBT and MFT at their early stage.

Key words : Himalaya, Finite element method, Major thrust, Incipient zone, MCT, MBT, MFT

1. Introduction

Himalaya is an active region where rapid crustal uplift occurred due to the convergence of Indian subplate beneath the Eurasian plate. The convergent plate motion is still occurring with different rates in the N-S direction along the Himalayan front shown in Fig. 1 (Minster and Jordan, 1978; Nakata *et al.*, 1990; Holt *et al.*, 1991). The northward convergence velocity was comparatively high at the early stage of collision, after this time, it is gradually decrease with 2 cm/a in the present time (Cattin and Avouac, 2000). As a result of the convergent plate motion numerous tectonic structures were formed in the Himalayas (Lyon-Caen and Molnar, 1983; Lave and Avouac, 2000). In this research, we simulated the formation of major thrusts (Main Central Thrust, Main Boundary Thrust and Main Frontal Thrust) on the profiles of Himalayas considering several convergent velocities after collision. The model profiles have been reconstructed with natural scale from Johnson (2002), where the major structures are MCT, MBT and MFT which were created from 40, 20 and 10 Ma, respectively. We treat the incipient zone of these thrusts as the area to explore their early developing stress state and element failure (fault).

In order to examine the development of major thrusts in Himalayas, we primarily calculate stress distribution and faults within the incipient zone of the future thrusts (MCT, MBT and MFT) by finite element method with Mohr Coulomb failure criterion. Then the simulated results are discussed and compared with the previous studies.

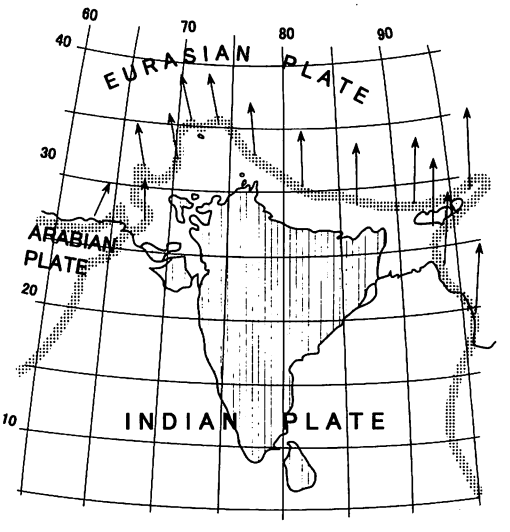

Fig. 1. The relative convergent motion between the Indian and Eurasian plates modified after Minster and Jordan (1978) and Nakata *et al.* (1990).

1.1. Geologic setting

The subduction of the Tethyan oceanic crust, which was located between India and Asia during Paleozoic and was followed by collision of continents, produced the structures and lithologies we see today in the Himalayas. Consequently, the mountains and surrounding regions are characterized by astound-

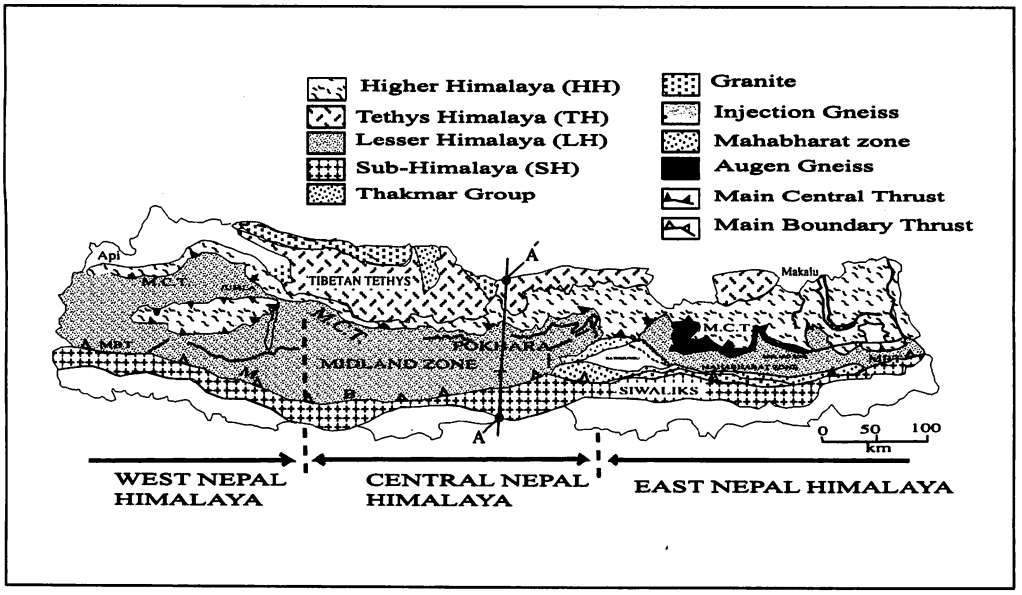

Fig. 2. Geological map of the central Himalaya. Slightly modified after Kano (1984).

ing complexity, representing a variety of lithologies and several phases of tectonic and deformational events (Windley, 1993). The Himalayas are divided into four litho-tectonic zones that occur in parallel belts. These zones consist of the Tethys Himalaya (TH), Higher Himalaya (HH), Lesser Himalaya (LH), and Sub-Himalaya (SH) shown in Fig. 2 (Kano, 1984). Tectonic environments within these zones also vary. Higher Himalayan range runs almost straight from Sikim to western Nepal. Several ranges such as Zanskar, Ladakh, and Kailas are situated in north of the HH (Sinha, 1987). Karakoram Range lies on the Tibetan side of the HH. South Tibetan Detachment System (STDS) represents a major system of north-dipping structural detachments along the boundary between the Higher Himalayan crystalline sequence and the Tethys Himalaya (Searle and Godin, 2003). The LH forms the footwall of the MCT in the southern part along the HH. The Lesser Himalayan zone is bounded by MCT in the north and by MBT to the south (Upreti, 1999). MBT separates the metapsammitic schists and phyllites of the LH from the conglomerates and sandstones of the SH (Arita *et al.*, 1984). Sub-Himalaya comprises Late Tertiary sediments which involve thin-skinned tectonics which is induced by thrusting of the Himalaya over the Indian basement (Pandey *et al.*, 1999).

1.2. Convergent rate of Indian plate after collision

The Himalayan mountain range occurred as a result of the Tertiary collision between the Indian and Asian plates. The collision divides into two stages (Le Pichon *et al.*, 1992). The first stage involves the convergence of the northward-drifting Indian subcontinent with a proto-Tibetan landmass during Late Cretaceous and Paleocene. The second stage involves formation of a fundamental crustal fracture within the Indian block during Late Eocene and Oligocene, and the underthrusting of the Indian subcontinent along this fracture from Miocene to Recent.

The convergent rate of Indian sub-plate under the Eurasian plate was comparatively fast in the initial stage and it has slowed down during the last 50 Ma (Trelor *et al.*, 1992). After the collision, India continued to move north resulting in crustal thickening, deformation and high topographic elevation. Sea floor palaeomagnetic stripe data show this movement rate about 15-20 cm/a (Trelor *et al.*, 1992). The continued continental collision decreased the rate about 5 cm/a (Tapponnier and Molnar, 1975 and 1979; Patriat and Achache, 1984; Nakata et al., 1990; Trelor et al., 1992; Upreti, 1999; Johnson, 2002).

Patriat and Achache (1984) have shown three successive phases for the Indo-Asia convergent rate. First, before anomaly 23 (52 Ma) India was drifting northward with a mean velocity of 15-20 cm/a. Then, between anomaly 23 and anomaly 13 (36 Ma)

Table 1. Post-collisional convergent rate and displacement between Indian and Eurasian plates.

model	convergent rate (cm/ a)	time span (Ma)	convergent displacement	fault
A	10	40-20	1500 m (for 15 ka)	MCT
B	5	20-10	1000 m (for 20 ka)	MBT
C	5	10-0	1000 m (for 20 ka)	MFT
D	2	0	700 m (for 35 ka)	

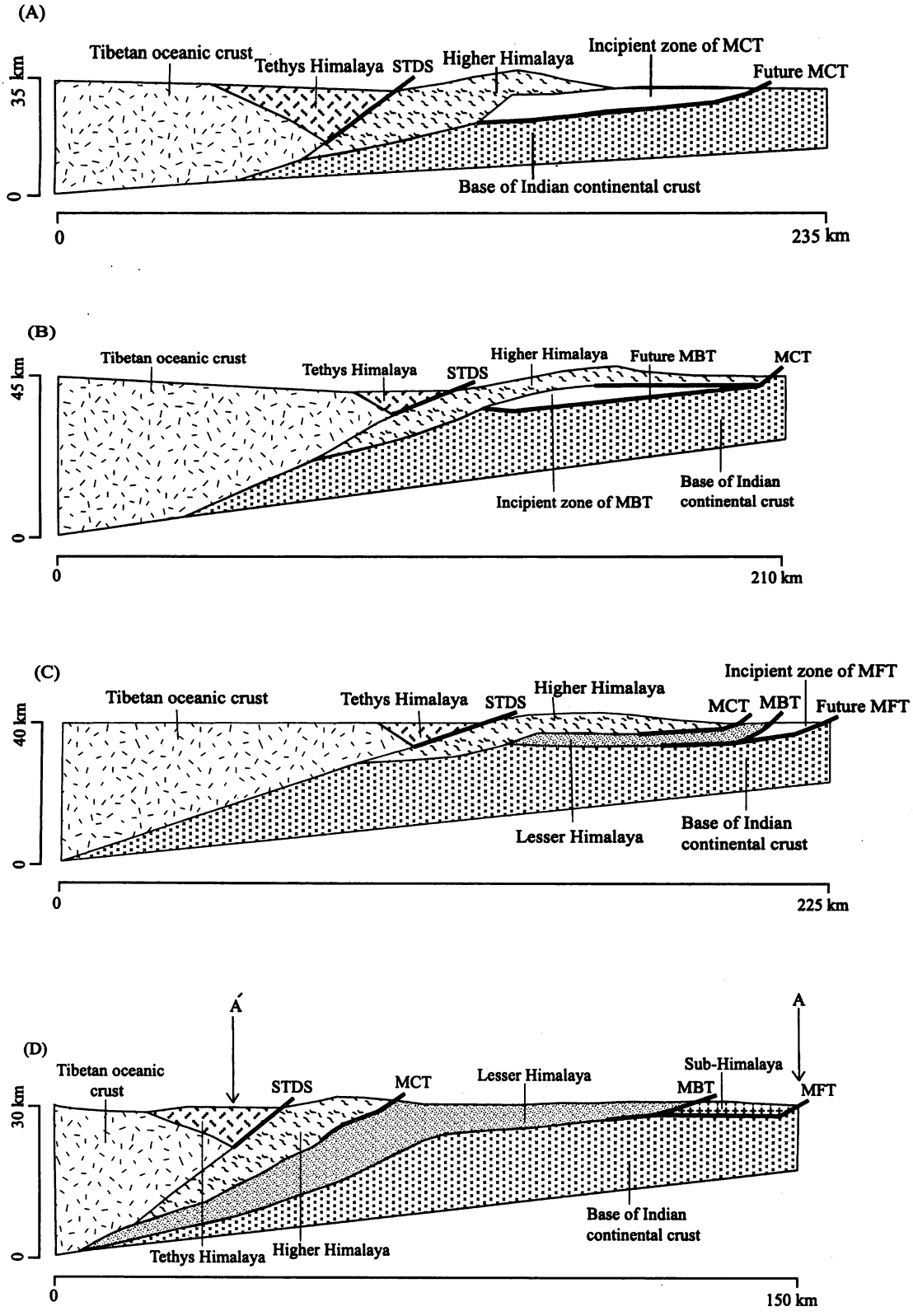

Fig. 3. Balanced geologic cross profiles of the central Himalaya. Slightly rearranged to natural scale after Johnson (2002). The profiles A, B, C and D are at 40, 20, 10 and 0 Ma, respectively. MCT= Main Central Thrust, MBT= Main Boundary Thrust, MFT= Main Frontal Thrust and STDS= South Tibetan Detachment System.

Table 2. Rock layer properties.

(2A)

rock layer	rock species	density (kg/ m³)	Poisson's Ratio	Young's Modulus (GPa)	cohesion (MPa)	friction angle (degree)
Tibetan oceanic crust	basalt	3000	0.27	80.0	52.00	51.0
Tethys Himalaya	limestone and sandstone	2700	0.23	70.0	35.00	37.0
Higher Himalaya	gneiss and granite	2800	0.25	75.0	45.00	40.0
Incipient zone of MCT	meta-sedimentary rocks	2200	0.20	67.5	30.00	23.0
Base of Indian continental crust	sandstone, gneiss and granite	2900	0.26	77.5	50.00	50.50

(2B)

rock layer	rock species	density (kg/m³)	Poisson's Ratio	Young's Modulus (GPa)	cohesion (MPa)	friction angle (degree)
Tibetan oceanic crust	basalt	2900	0.27	77.5	47.50	52.0
Tethys Himalaya	limestone and sandstone	2600	0.23	67.5	34.00	40.5
Higher Himalaya	gneiss and granite	2700	0.25	72.5	42.50	42.0
Incipient zone of MBT	meta-sedimentary rocks	2100	0.20	65.5	29.00	24.0
Base of Indian continental crust	sandstone, gneiss and granite	2800	0.26	75.0	45.00	51.0

(2C)

rock layer	rock species	density (kg/ m³)	Poisson's Ratio	Young's Modulus (GPa)	cohesion (MPa)	friction angle (degree)
Tibetan oceanic crust	basalt	2800	0.27	75.0	45.00	53.0
Tethys Himalaya	limestone and sandstone	2600	0.23	65.0	32.00	42.0
Higher Himalaya	gneiss and granite	2650	0.25	70.0	37.00	45.0
Lesser Himalaya	phyllite	2500	0.21	62.0	31.00	37.0
Incipient zone of MFT	clastic sedimentary rocks	2000	0.20	60.0	27.00	25.0
Base of Indian continental crust	sandstone, gneiss and granite	2700	0.26	72.0	42.00	52.0

(2D)

rock layer	rock species	density (kg/ m³)	Poisson's ratio	Young's modulus (GPa)	cohesion (MPa)	friction angle (degree)
Tibetan oceanic crust	basalt	2700	0.27	72.5	43.00	55.0
Tethys Himalaya	limestone and sandstone	2450	0.23	60.0	31.00	43.5
Higher Himalaya	gneiss and granite	2600	0.25	65.0	35.00	47.0
Lesser Himalaya	phyllite	2400	0.21	55.0	29.00	36.0
Sub-Himalaya	Sandstone and siltstone	2200	0.20	40.0	26.00	20.0
Base of Indian continental crust	sandstone, gneiss and granite	2650	0.26	70.0	40.00	52.5

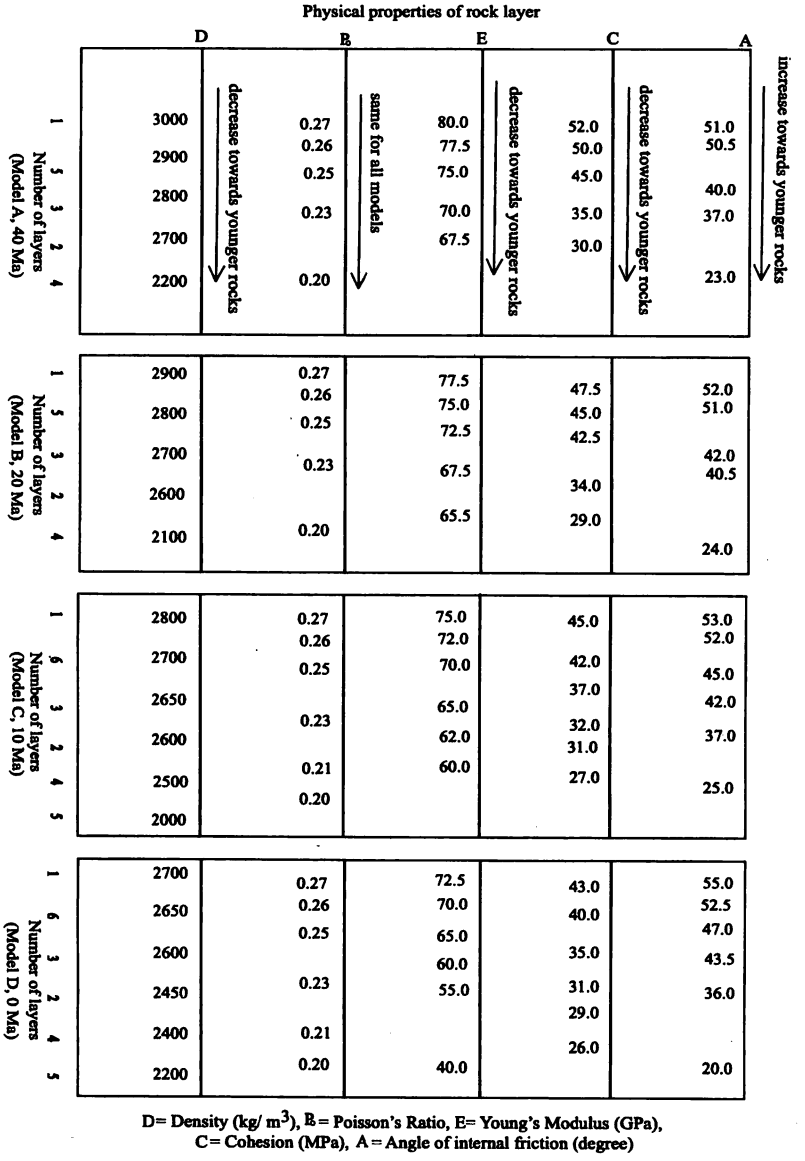

Fig. 4. Rock layer properties of models A to D.

the motion of India became rather erratic showing several changes in direction and the mean northward velocity was reduced to less than 10 cm/a. Finally, anomaly 5 (10 Ma) India resumed a stable northward direction of convergence with respect to Eurasia with a rate of 5 cm/a. The present convergence rate across the Himalayan range is 2 cm/a (Cattin and Avouac, 2000). Based on the above discussions, we summarize the convergent rates during collisional period on Table 1 which are used for the present simulation.

2. Modeling

2.1. Profile models

We have produced a series of 2D finite element models considering the geologic profiles in the central Himalaya shown by line A-A′ in Fig. 2. The models A, B, C, and D (Fig. 3) are rearranged with natural scale for our simulation from Johnson's profiles (2002). Models A, B and C are prepared to examine the idea that the MCT, MBT and MFT are created from the incipient zones assumed by Johnson (2002). Model D presents the present Himalayan profiles with which we can compare the presently observed stress and fault. They are divided into a number of triangular elements with three nodes. The total number of elements, nodes, size and boundary condition of the four models varies from one another are shown in Fig. 5. The models are simulated under the rock layer properties (density, Poisson's ratio, Young's modulus, cohesion and angle of internal friction) and boundary conditions (convergent displacement) to simulate the stress distribution and to recognize the failured elements (fault) area in the models by the proximity to failure (P_f) under the Mohr Coulomb failure criterion.

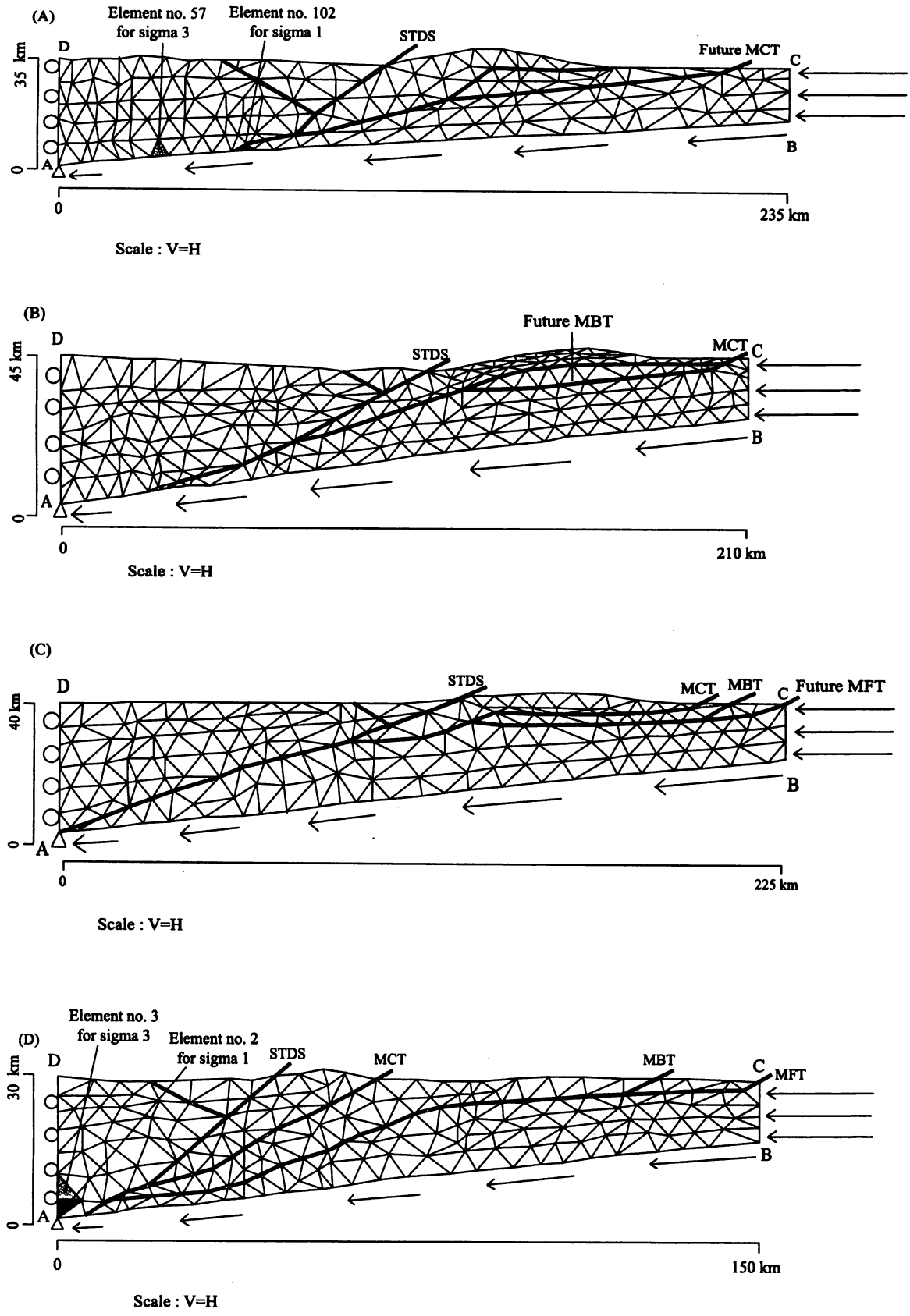

Fig. 5. Architecture and boundary condition of finite element grid models A to D in natural scale (V=H). Node A is fixed. The nodes of left edge (AD) move vertically. Different displacement to left is imposed perpendicular to right boundary (BC). Along the base (AB) of all models, displacement is proportionally distributed to the distance from the point A. All arrows indicate the direction and magnitude of displacement. Elements 102 and 57 in model A and elements 2 and 3 in model D show the maximum values of σ_1 and σ_3 .

2.2. Rock layers of model profiles

The Himalayan profiles which we used, consist of five or six rock layers shown in Fig. 3. The Higher Himalaya composed of gneiss and schist which form the basement of the Tethys Himalaya with various kinds of leucogranite from Eocene to Middle Miocene and later (Searly *el al.*, 1987). The age of Tethys Himalaya ranges from Cambrian to Tertiary period. Lesser Himalaya comprises relatively high-grade phyllite whose age is still controversial (Kaneko, 1997; Upreti, 1999). Sub-Himalaya comprises of Neogene to Quaternary fluvial sedimentary rocks (Kano, 1984; Upreti, 1999). The incipient zones of MCT, MBT and MFT are covered by the metasedimentary and clastic sedimentary rocks, respectively which are derived from erosion of the frontal part of Himalayas. Tibetan oceanic crust composed of basalt.

We consider with regards to the rock layer properties that there is a tendency. The older the rock layer is, the larger the rock properties (density, Young's modulus and cohesion) are, while the lesser the friction angle is; and Poisson's ratio is considered constant shown in Fig. 4. The rock layer properties are listed in Table 2.

2.3. Boundary condition

Boundary condition is important for evaluating the stress field and fault pattern. The boundary conditions are same for four models except for the value of displacement. The different convergent displacements, which derived from the different convergent velocities multiplied by period (100-35000 years), are imposed perpendicular to the right-side wall (BC) as already mentioned in Table 1 and Fig. 5. Along BC, displacement is free. We used the convergent rate 10 cm/a for model A, 5 cm/a for model B and C and 2 cm/a for model D to estimate the boundary displacements 1500 m (for 15 ka) in model A, 1000 m (for 20 ka) in model B and C and 700 m (for 35 ka) in model D and calculated stress distribution in the models. The left side edge (AD) is fixed horizontally. Node A is fixed. As the value of displacement is given proportional to the distance from the point A along bottom line AB, the imposed displacements are shown by arrows in Fig. 5. These imposed displacements are vectors which have both components of horizontal and vertical . The upper boundary (CD) is free, so as the earth's surface.

3. Results

3.1. Stress distribution

Stress field of four models are almost similar to each other, though their convergent displacement boundary conditions are different. The stress pattern shows the compressive nature of principal stresses in all part of the models (Fig. 6). No tensional stress observed in the models. The magnitude and orientation of the principal stresses primarily depend on boundary condition and rock layer properties. It is always difficult to decide the value of rock properties. Thus, we examine a lot of models changing the values of rock layers property on the results. The values are finally fixed and listed in Table 2. The displacement imposed as boundary condition hardly affects the tendency of stress distribution. The direction of maximum principal stress σ_1 is almost the same for all the models, whereas σ_1 deviated slightly from the horizontal along the bottom part of the Tibetan oceanic crust, Higher Himalaya, Lesser Himalaya and the base of Indian continental crust. Magnitudes of compressive stresses σ_1 and σ_3 are increasing gradually with depth to reach the highest limit along the basal part of models (Fig. 6). The maximum value of compressive stresses σ_1 is 1061.71 MPa (element no. 102) and σ_3 739.47 MPa (element no. 57) in model A. Those values decrease to 919.08 MPa (element no. 2) and 609.66 MPa (element no. 3) in model D.

3.2. Distribution of failured finite element

To estimate the role of displacement on forming the failured element under plane strain condition, we calculate the proximity to failure (P_f) which is proposed by Melosh and Williams (1989), from the principal stresses σ_1 and σ_3. The method how to calculate P_f is described by Howladar and Hayashi (2003). We determined the failured element considering the proximity to failure (P_f) under the Mohr Coulomb failure criterion. If the value of P_f is equal or larger than 1.0, failure occurs.

Simulation shows that failured elements take mostly place within the Thethys Himalaya, Higher Himalaya, incipient zone of major thrusts, Lesser Himalaya and Sub-Himalaya from Late Eocene to present (Fig. 7). The compressive stress σ_1 oriented horizontally in the Thethys Himalaya, Higher Himalaya, incipient zone of MCT, MBT and MFT, Lesser Himalaya and Sub-Himalaya. Thrust faults are expected which are highly concentrated within the incipient zones than other rock layers for three models A, B and C (Fig. 7).

4. Discussions

4.1. Formation of major thrusts

The major thrusts are the MCT, MBT and MFT in Himalayas which are produced by the continual northward compressional movement of Indian sub-plate. Lyon-Caen and Molnar (1983) and Johnson (2002) proposed that the MCT, MBT and MFT were created at 40, 20 and 10 Ma, whereas their formation was completed at 20, 10 and 0 Ma, respectively. In the present simulation, we observed that the thrust faults are highly concentrated within the incipient zones of such thrusts (Fig. 7). We believe, that the simulated thrust faults within these zones must have been responsible for the early development of these thrusts.

Active faults in the Himalayas are MCT and MBT (Joshi and Patel, 1997) and MFT (Lyon-Caen and Molnar, 1983; Lave

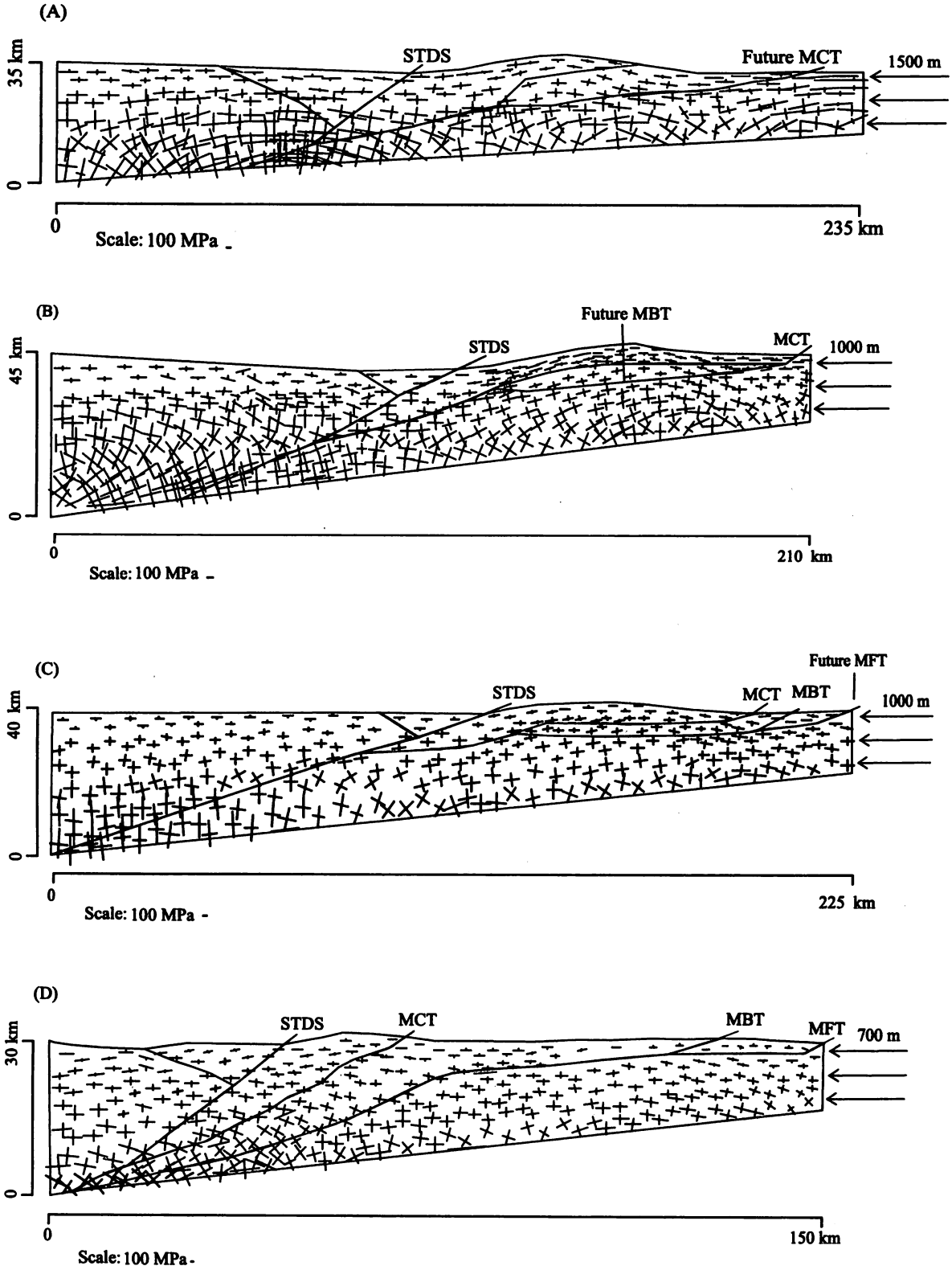

Fig. 6. Distribution of simulated principal stresses σ_1 and σ_3 of models A to D.

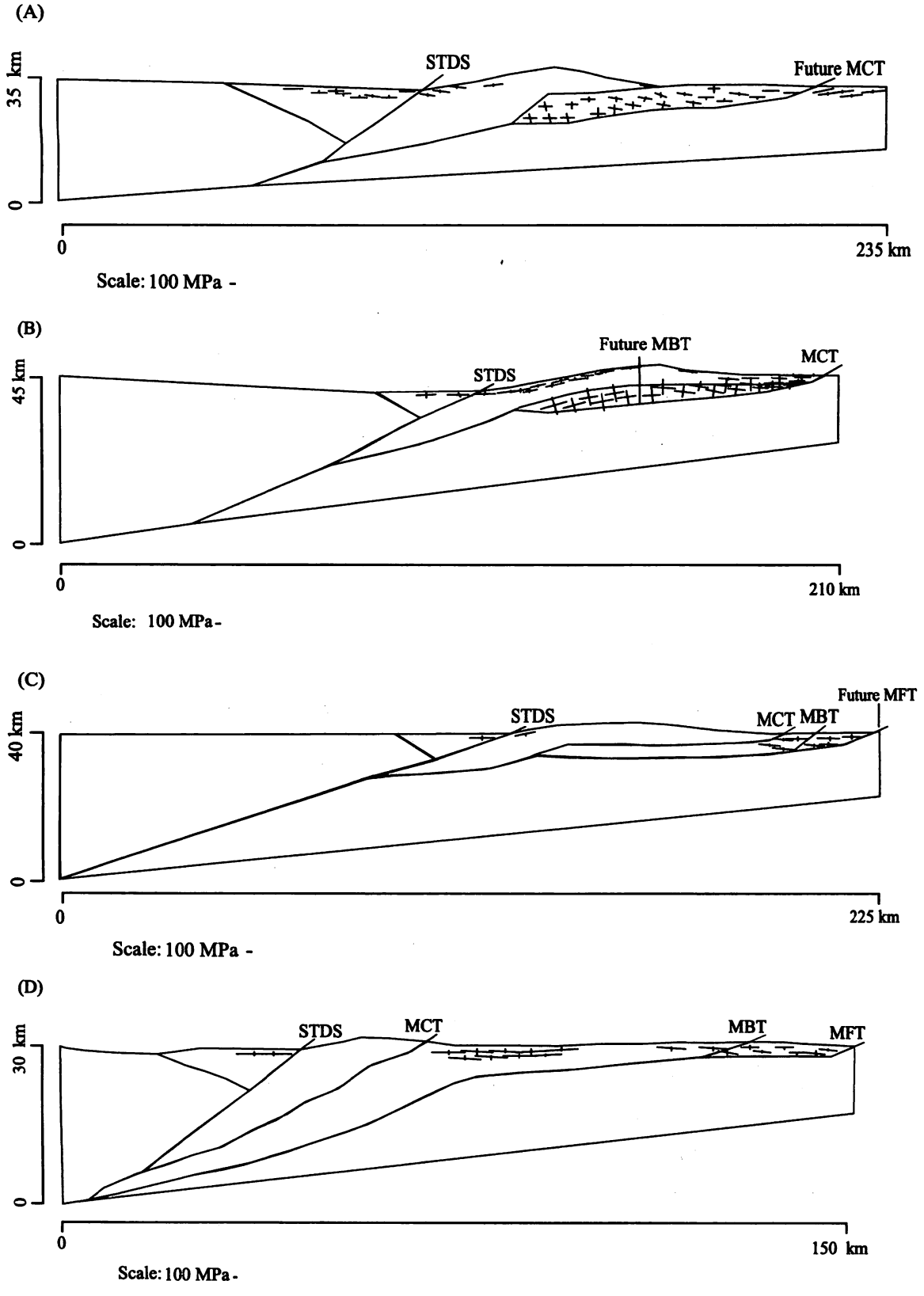

Fig. 7. Determination of fault based on the calculated stress field under Coulomb-Mohr criterion of models A to D.

and Avouac, 2000). MCT is thought to be active during Miocene (Hodges *et al.*, 1996). Slip movement in south of the MCT occurred along the MBT (Meigs *et al.*, 1995) in Late Miocene. MFT is now active (Yeats et al., 1992). These active thrusts are also the direct indicator of the crustal movements due to the collision between the Indian and Eurasian plate (Nakata *et al.*, 1984).

4.2. Elastic rheology

According to the plate tectonic theory, the upper half of the lithosphere is referred to as elastic lithosphere (Turcotte and Schubert, 1982). The reason for considering the elastic behavior of lithosphere is to understand the stress state and their relevance to form the faults in the study area. It is well known that the elastic deformation, even if small, governs the initiation of fault in nature (Yin, 1993). Thus, our elastic models under plane strain condition justified to consider the fault distribution. As once we assume elasticity, the values of stress are severally controlled by elastic constants, the rock layer's property should be carefully chosen (Table 2). As the value of elastic constants varies with depth and time span, the average value is adopted for the simulation.

4.3. Comparison with the previous studies

Simulated compressive stress fields coincide with continuous NS compressional influences of Indian plate to the Himalayan profiles shown in Fig. 6. The failured elements predicted by our simulation in models A, B and C are recognized within the Tethys Himalaya, Higher Himalaya, incipient zones and Lesser Himalaya, where compressive stress oriented horizontally which leads to the formation of the thrust faults in the proposed models (Fig. 7). Searle (1983a, 1986) and Searly *et al.* (1987) reported that the progressive south directed thrust fault developed after the collision during middle Tertiary period along central part of Himalaya which is the explanation of simulated thrust fault for model A, B and C. After Eocene, thrust deformation spreads southward. Consequently, thrust faults are observed in the Tethys Himalaya, then in the frontal part of MCT, MBT and finally along the MFT at the present stage (Fig. 7 D). These present stage thrust faults seem to be associated with the major intra-continental thrust MCT, MBT and MFT (Nakata, 1989). The existence of such fault in the frontal part of the Himalayas is in agreement with neotectonic movements along the MFT in the Nepal Himalaya (Nakata *et al.*, 1984). The successive development of fault from Late Eocene to present shows the close relation with the transformation of active subduction of Indian continental crust in the Himalayas during the post-collisional period (Johnson, 2002). Furthermore, the developments of a large number of thrust faults within the incipient zones of such future thrusts are the evidences of early development of the MCT, MBT and MFT.

5. Conclusion

We simulate a series of finite element model to show the development of major thrusts on the profiles of central Himalaya after collision. Simulated compressive principal stresses show tendency to decrease their magnitude towards the shallower region where σ_1 stress axis rotated horizontally of four models. This rotation of the principal stress axis decides the direction of thrust faults, while the stress difference σ_1-σ_3 generates these faults. The thrust faults produced in the models A, B and C are recognized within the Thethys Himalaya, Higher Himalaya, incipient zones and Lesser Himalaya. After 10 Ma, deformation spreads southward across the Higher Himalaya to the outer Himalayas. Consequently, the present stage thrust faults show the high concentration towards south from the Thethys Himalaya and the frontal part of MCT, MBT finally along the MFT that provides a good agreement with sequential southward thrust development in the Himalayan orogeny. We observed the thrust fault in the frontal part of Himalaya which might be associate with neotectonic movements along the MFT of the area.

Acknowledgments

The authors appreciate the help by T. Morishita for preparing the figures. We thank also anonymous reviewers for their critical comments, which improved the manuscript considerably. M.F.H. is highly grateful to the Heiwa Nakajima Foundation for the financial support to this work. He is also indebted to S. Afroz for her valuable discussions and continuous encouragement to prepare the early stage manuscript.

References

Arita, K., Shiraishi, K. and Hayashi, D. (1984) Geology of western Nepal and a comparison with Kumaun, India. *Bulletin, Faculty of Science, Hokkaido University*, Ser. IV. vol. 21 no. 1, pp. 1-20.

Cattin, R. and Avouac, J. P. (2000) Modeling mountain building and the seismic cycle in the Himalaya of Nepal. *Journal of Geophysical Research*, vol. 105, no. B(6), pp. 13389-13407.

Hodges, K.V., Parrish, R. R. and Searle, M. P. (1996) Tectonic evolution of the central Annapurna Range, Nepalese Himalayas. *Tectonics*, vol. 15, pp. 1264-1291.

Holt, W. E., Ni, J. F., Wallace, T. C. and Haines, A. J. (1991) The active tectonics of the Eastern Himalayan syntaxis and surrounding regions. *Journal of Geophysical Research*, vol. 96, pp. 14595-14632.

Howladar, M. F. and Hayashi, D. (2003) Numerical fault simulation in the Himalaya with 2 D finite element method. *Journal of Polar Geoscience*, vol. 16, pp. 243-258.

Joshi, A. and Patel, R. C. (1997) Modeling of active lineaments for predicting a possible earthquake scenario around Dehradun, Garhwal Himalaya, India. *Tectonophysics*, vol. 283, pp. 289-310.

Johnson, M. R. W. (2002) Shortening budgets and the role of continental subduction during the India-Asia collision. *Earth-Science Reviews*, vol. 59, pp. 101-123.

Kaneko, Y. (1997) Two-step exhumation model of the Himalayan metamorphic Belt, central Nepal. *Journal of Geological Society of Japan*, vol. 103(3), pp. 203-226.

Kano, T. (1984) Geology and structure of the Main Central Thrust zone of the Annapurana range, Central Nepal Himalayas. *Journal of Geological Society of Japan*, vol. 2, pp. 31-50.

Lave, J. and Avouac, J. P. (2000) Active folding of fluvial terraces across the Siwaliks Hills, Himalayas of central Nepal. *Journal of Geophysical Research*, vol. 105, pp. 5735-5770.

Le Pichon, X., Fournier, M. and Jolivet, J. (1992) Kinematics, topography, shortening and extrusion in the India-Asia collision. *Tectonics*, vol. 11, pp. 1085-1089.

Lyon-Caen, H. and Molnar, P. (1983) Constraints on the structure of the Himalaya from an analysis of gravity anomalies and a flexural model of the lithosphere. *Journal of Geophysical Research*, vol. 8, no. B(10), pp. 8171-8191.

Melosh, H. J. and Williams, C. A. (1989) Mechanics of Graben formation in crustal rocks: a Finite element analysis. *Journal of Geophysical Research*, vol. 94, pp. 13961-13973.

Meigs, A. J., Burbank, D.W. and Beck, R. A. (1995) Middle-late Miocene [>10 Ma] formation of the Main Boundary Thrust in the Western Himalaya. *Geology*, vol. 23, pp. 423-426.

Minster, J. B. and Jordan, T. H. (1978) Present day plate motions. *Journal of Geophysical Research*, vol. 83, pp. 5331-5354.

Nakata, T., Iwata, S., Yamanaka, H., Yagi, H. and Maemoku, H. (1984) Tectonic landforms of several active faults in the western Nepal Himalayas. *Journal of Nepal Geological Society*, vol. 4, pp. 177-200.

Nakata, T. (1989) Active faults of the Himalaya of India and Nepal. *Special paper Geological Society of America*, vol. 232, pp. 243-264.

Nakata, T., Otsuki, K. and Khan, S. M. (1990) Active faults, stress field and plate motion along the Indo-Eurasian plate boundary. *Tectonophysics*, vol. 181, pp. 83-95.

Pandey, M. R., Tandukar, R. P., Avouac, J. P., Vergne, J. and Heritier, T. (1999) Seismo-tectonics of the Nepal Himalaya from a local seismic network. *Journal of Asian Earth Science*, vol. 17, pp. 703-712.

Patriat, P. and Achache, J. (1984) India-Eurasia collision chronology has implications for crustal shortening and driving mechanism of plates. *Nature*, vol. 311, pp. 615-621.

Searle, M. P. (1983a) Stratigraphy, structure and evolution of the Tribetan-Tethys zones in Zanskar and the Indus suture zone in the Ladakh Himalaya. *Royal Society of Edinburg Transactions, Earth Sciences*, vol. 73, pp. 205-219.

Searle, M. P. (1986) Structural evolution and sequence of thrust in the Higher Himalaya, Tibetan-Tethys and Indus suture zone of Zanskar and Ladakh, western Himalaya. *Journal of structural Geology*, vol. 8, pp. 923-936.

Searle, M. P., Windley, B. F., Coward, D. J. W., Rex, A. J., Rex, D., Tindong Li, Xuchang, X., Jan, M. Q., Thakur, V. C. and Kumar, S. (1987) The closing of Tethys and the tectonics of the Himalaya. *Geological Society Bulletin of America*, vol. 98, pp. 678-701.

Searle, M. P. and Godin, L. (2003) The South Tibetan Detachment and the Manaslu Leucogranite: A Structural Reinterpretation and Restoration of the Annapurna-Manaslu Himalaya, Nepal. *Journal of Geology*, vol. 111, pp. 505-523.

Sinha, A. K. (1987) Tectonic zonation of the central Himalayas and the crustal evolution of collision and compressional belts. *Tectonophysics*, vol. 134, pp. 59-74.

Tapponnier, P. and Molner, P. (1975) Cenozoic tectonics of Asia, effects of continental collision. *Science*, vol. 189, pp. 419-426.

Tapponnier, P. and Molner, P. (1979) Active faulting and Cenozoic tectonics of the Tien Shen, Mongolia and baikal region. *Journal of Geophysical Research*, vol. 84, pp. 3425-3459.

Trelor, P. J., Coward, M. P., Chambers, A. F., Izatt, C. N. and Jackson, K. C. (1992) Thrust geometries, interferences and rotations in the Northwest Himalaya. *Thrust Tectonics*, edited by McClay, pp. 325-342.

Turcotte, D. L. and Schubart, G. (1982) *Geodynamics: Applications of Continuum Physics to Geological problems*. John Wiley and Sons, 450p.

Upreti, B. N. (1999) An overview of the stratigraphy and tectonics of the Nepal Himalaya. *Journal of Asian Earth Science*, vol. 17, pp. 577-606.

Windley, B. F. (1989) Metamorphism and tectonics of the Himalayas. *Journal of Geological of Society of London*, vol. 140, pp. 849-866.

Yeats, R. S., Nakata, T., Farah, A., Fort, M., Mirza, M. A., Pandey, M. R. and Stein, R. S. (1992) The Himalayan Frontal Fault System. *Annales Tectonicae*, vol. 6, pp. 85-98.

Yin, A. (1993) Mechanics of wedge shaped fault blocks an elastic solution for compressional wedge. *Journal of Geophysical Research*, vol. 98, pp. 14245-14256.

要　旨

有限要素法によるヒマラヤの主要スラストのシミュレーション

：M. F. Howladar*・林　大五郎*

大規模な地殻の運動によって出現したヒマラヤ山系はインドプレートとユーラシア大陸プレートとの衝突によりもたらされた．ここに取り上げた一連の弾性有限要素モデルは中央ヒマラヤの主要スラスト（MCT，MBT，MFT）の発達過程を表している．Johnson（2002）によって作成された中央ヒマラヤのバランス地質断面図を多少修正したものを平面ひずみの条件のもとで使用した．インドプレートの速度を40Maでは10cm／年，20Maでは5cm／年，10Maでは2cm／年に設定した．シミュレーションの結果，水平圧縮応力σ_1はテーチスヒマラヤ，高ヒマラヤ，低ヒマラヤ，サブヒマラヤ，そしてMCT，MBT，MFTの萌芽地帯にスラストを生じさせた．特に将来MCT，MBT，MFTとなる萌芽地帯全体でのスラストの発生する領域の占める割合は高い．

キーワード：ヒマラヤ，有限要素法，主要スラスト，萌芽地帯，MCT，MBT，MFT

*琉球大学理学部物質地球科学科